WindSat Calibration and Geophysical Parameter Estimation

Christopher S. Ruf, Shannon T. Brown, Ying Hu and Hirofumi Kawakubo
University of Michigan, Ann Arbor, MI, USA
734-764-6561 (V), 734-936-0503 (F), cruf@umich.edu (E)

***Abstract* – Three aspects of WindSat performance are presented. 1. End-to-end system calibration is tested by comparisons between WindSat measurements and a robust model of the Earth T_B using the vicarious cold reference method. 2. In an effort to determine probable causes for any calibration biases or scale errors that are identified, a refined Antenna Pattern Correction algorithm has been developed that includes main reflector aperture illumination and edge diffraction effects, in addition to the feed spillover effects that are already accounted for in WindSat's nominal flight processing algorithm. 3. A wind vector retrieval algorithm has been developed that is based on an empirical geophysical model function relating the four Stokes components of ocean surface emissivity to wind speed and direction. In order to implement an emissivity-based retrieval, decomposition of the radiative transfer equation is performed into surface and atmospheric contributions.**

keywords - microwave radiometer, polarimetry, wind retrieval

I. INTRODUCTION

WindSat was successfully launched in January 2003 on the Coriolus spacecraft. WindSat operates at 6.8, 10.7, 18.7, 23.8, and 37 GHz with a conically scanned 1.83 m offset parabolic reflector antenna. The 10.7, 18.7, and 37.0 GHz channels are fully polarimetric, directly measuring the incident antenna temperature (T_A) at the six polarization states: vertical (T_V), horizontal (T_H), +45° slant linear (T_P), –45° slant linear (T_M), left hand circular (T_L) and right hand circular (T_R). From these measurements, the 3rd and 4th Stokes brightness temperatures (T_Bs) can be derived, as $T_3 = T_P - T_M$ and $T_4 = T_L - T_R$. WindSat is the first fully polarimetric microwave radiometer in space [Gaiser, 1998].

WindSat is intended to remotely sense the speed and direction of near surface winds over the ocean. To do so requires that residual biases in the measurement of T_3 and T_4 be kept extremely low – on the order of 0.1 K or lower. This, in turn, requires that non-common mode biases in the calibration of T_P relative to T_M and in T_L relative to T_R be kept at least as low. Two independent methods have been developed and implemented to characterize and correct for both common mode and non-common mode biases in T_B calibration at all relevant polarizations. End-to-end system calibration is tested by comparisons between WindSat measurements and a vicarious cold ocean emission model. The most likely sources of calibration bias are inaccuracies in the Antenna Pattern Correction (APC) algorithm which removes antenna sidelobe contributions to the measured T_A and extracts the T_B in the mainbeam. As an independent assessment of calibration bias, a refined APC algorithm has been developed that includes main reflector aperture illumination and edge diffraction effects, in addition to the feed spillover effects that are already accounted for in the flight processing algorithm.

The accurate retrieval of surface wind speed and direction requires that the observed T_B be decomposed into its component sources: atmospheric upwelling and downwelling and ocean surface emission. A candidate decomposition algorithm has been developed which estimates the optical depth and upwelling and downwelling T_B of the atmosphere at each WindSat frequency, as well as the ocean surface emissivity at all pertinent polarizations, including ε_3 and ε_4. Retrieval of the fully polarimetric ocean surface emissivities form the basis for a robust, all-weather, retrieval algorithm for wind speed and direction.

II. VICARIOUS COLD REFERENCE

A stationary statistical lower bound on microwave T_B observations over the ocean can be utilized to produce a Vicarious Cold Reference (VCR) brightness against which the end-to-end calibration of a satellite radiometer can be compared [Ruf, 2000]. The VCR method can be used to check a number of characteristics of instrument calibration. Two are illustrated here for the case of WindSat. A large ensemble of WindSat T_B observations are first assembled, covering a span of approximately 2 weeks. Only open ocean data are used and T_Bs are binned according to azimuth scan position. For

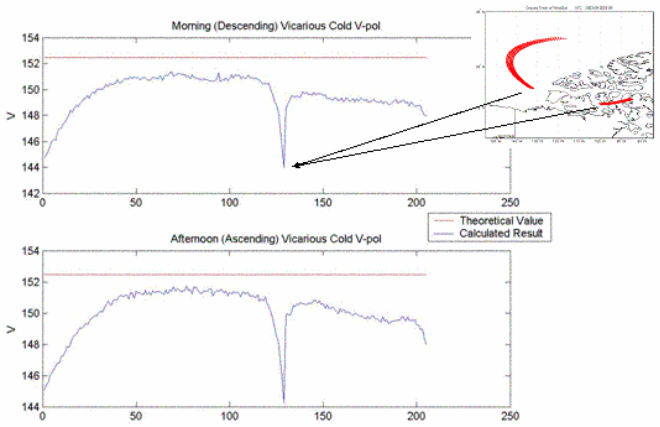

Fig. 1. Vicarious Cold Reference brightness temperature for 6.8 GHz V-pol channel versus azimuth scan position. The dependence on scan position most likely results from variable interference by calibration hardware. Insert shows equivalent swath position on Earth. Horizontal red line is theoretical Earth VCR TB. The offset of the measurements represents a calibration bias.

each scan position, a histogram of T_Bs is assembled and extrapolated in order to estimate the highest T_B below the measurements with a zero probability of occurrence. This is the VCR. Results are shown in Fig. 1 for the 6.8 GHz V-pol channel. Two characteristics of instrument calibration are noteworthy. The sharp drop in VCR near scan position 129 is most likely due to partial blockage and scattering of the feed horn pattern by WindSat's hot reference absorber. The absorber is sampled between scan positions 129 and 130. The VCR also rolls off near samples 1 (first sample) and 205 (last sample). The cold sky reflector is sampled between these. The more gradual changes in VCR with scan position away from the calibration regions is probably due to known variations in Earth incidence angle with scan position. The theoretical VCR values vary with incidence angle in a manner consistent with these observations. The horizontal red lines in Fig. 1 represent the VCR values corresponding to the average of all observed incidence angles. Observations are consistently biased low. Similar analysis of the 6.8 GHz H-pol T_Bs show a positive bias. This suggests that the correction for cross-polarized contamination is incomplete.

III. ANTENNA PATTERN CORRECTION MODELING

WindSat's Antenna Pattern Correction (APC) algorithm attempts to deconvolve sidelobe and cross-polarized contamination from the measured antenna temperatures (T_A) to produce the co-polar, main beam only, brightness temperatures. An example of one method for estimating the accuracy of the correction for cross-pol contamination was discussed in Section II above. Here, we estimate the level of sidelobe contamination and construct a first order deconvolution algorithm to correct for it. The overall antenna radiation pattern can be decomposed in the following manner (illustrated in Fig. 2). The feed horn pattern defines an aperture illumination field on the main reflector. A portion of the feed horn pattern also spills over the main reflector and represents power entering from the far sidelobes of the overall radiation pattern. The main reflector illumination can be transformed into a far field radiation pattern . This forms the overall main beam and near sidelobe structure. Finally, the current ring

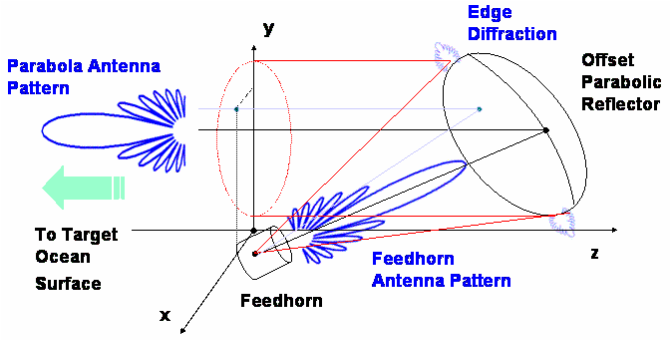

Fig. 2. Conceptual representation of factors contributing to overall WindSat antenna pattern. Only the feedhorn spillover has been previously accounted for in the WindSat APC agorithm

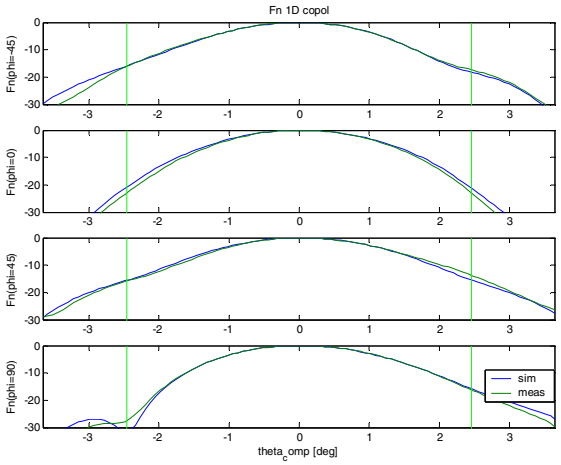

Fig. 3. Principle plane and ± 45° simulated and measured main beam antenna patterns at 6.8 Hz, V-pol, optimized by feed horn phase pattern.

generated around the outer edge of the main reflector will produce a ring diffraction lobe generally focused in the opposite direction from the main beam.

An antenna radiation model has been constructed that includes all of these effects and produces estimates of the overall antenna radiation. Inputs to the model are the feed horn amplitude radiation pattern and the physical geometry of the feeds and main reflector. A free parameter of the model is the phase of the feed horn radiation pattern, which was not adequately measured prior to launch. The phase pattern is adjusted in the model to force a best fit agreement between the predicted and measured main beam pattern. An example of the result is shown in Fig. 3 at 6.8 GHz, V-pol. Once the model has been adjusted to match the measured main beam pattern, it can be used to estimate the contributions to T_A from all far sidelobe beam fractions. The far sidelobe contributions can then be subtracted off in the first order deconvolution stage of the APC algorithm.

IV. OCEAN SURFACE EMISSIVITY EMPIRICAL MODEL FUNCTION

The T_B observed by WindSat at frequency, *f*, and polarization, *p*, can be represented as

$$TB_{f,p} = T_B^{UP} + \left(1-\varepsilon_{f,p}\right)\times \left[T_B^{DN} + T_c e^{-\tau\sec\theta}\right]e^{-\tau\sec\theta} + \varepsilon_{f,p} SST e^{-\tau\sec\theta} \quad (1)$$

where τ is the optical depth of the atmosphere, $\sec\theta$ approximates the slant path length through the atmosphere at incidence angle θ, $T_B^{UP,DN}$ are the upwelling and downwelling T_Bs of the atmosphere, SST is the sea surface temperature (in K) and $\varepsilon_{f,p}$ is the ocean surface emissivity. The surface emissivity can be solved in (1) provided the atmospheric compo-

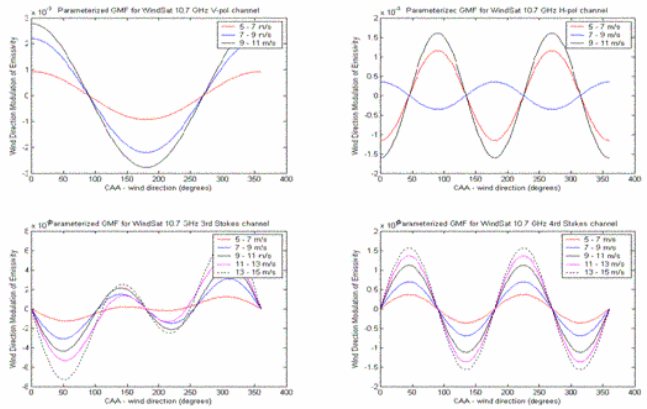

Fig. 4. Harmonic best fit of measured ocean surface emissivity at 10.7 GHz versus relative azimuthal look direction for different wind speeds between 5 and 15 m/s. V-pol (upper left), H-pol (upper right), 3rd Stokes (lower left), 4th Stokes (lower right).

nents are known. They are estimated directly from the V-pol observations using a physically based non-linear multi-parameter least squares retrieval algorithm that simultaneously solves for atmospheric water vapor burden, cloud liquid water and ocean surface winds. Only the V-pol channels are used to minimize the sensitivity of the algorithm to effects of wind speed and direction. The water vapor and cloud liquid are used to determine the atmospheric optical depth that is needed to invert (1).

The ocean surface emissivity is extracted from the measurements by inverting (1) for a large data base of matchups with NDBC buoys. The wind speed and direction provided by the buoys is then used to construct empirical model functions of ocean surface emissivity versus wind speed and direction. Best fit first and second harmonic functions of the relative wind direction are shown in Fig. 4 for the four 10.7 GHz Stokes emissivities. These empirical models are in good general agreement with earlier published results derived from aircraft observations [Yueh, 1997; Yueh *et al.*, 1999]

In order to develop a wind vector retrieval algorithm using WindSat T_Bs, it is necessary to parameterize the harmonic coefficients of the model function with respect to wind

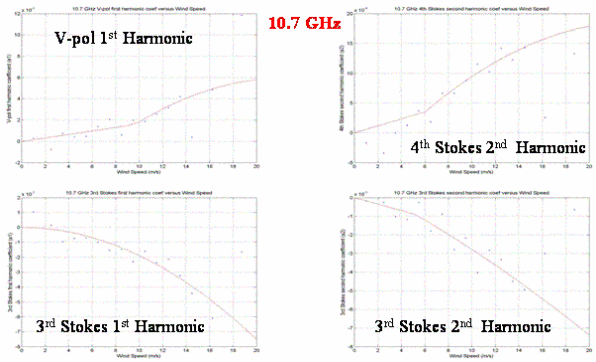

Fig. 5. Empirical geophysical model function relating the 1st and 2nd harmonics of 10.7 GHz ocean surface emissivity's dependence on wind relative azimuth direction versus wind speed.

speed. An example of this parameterization is shown in Fig. 5 at 10.7 GHz for some of the stronger harmonics at various polarizations. Similar parameterized empirical model functions have been developed at all frequencies and polarizations for use in the wind vector retrieval algorithm.

V. WIND VECTOR RETRIEVAL

A wind vector retrieval algorithm has been developed based on the empirical emissivity model functions. The algorithm uses the following processing steps. 1. V-pol T_Bs are used to retrieve atmospheric column water vapor and integrated cloud liquid water. An ancillary simultaneous estimate of ocean surface wind speed is also made at this stage, but it is not used in subsequent processing steps. 2. Atmospheric optical depth is estimated for each WindSat channel using the retrieved water vapor and cloud liquid. A latitude dependent database of effective atmospheric radiating temperatures, $T_B^{UP,DN}$, derived from a global ensemble of RaOb profiles, is combined with the optical depth to estimate the upwelling and downwelling atmospheric brightness, according to

$$T_B^{UP,DN} = \left(1 - e^{-\tau \sec\theta}\right) T_{eff}^{UP,DN} \qquad (2)$$

3. All polarimetric components of the Stokes emissivity vector are solved by inverting (1) at each WindSat channel. 4. The two dimensional state space of possible wind speeds and directions is subdivided into small cells. For each wind vector cell, all polarimetric components of emissivity at each WindSat frequency are computed using the empirical model function. The RMS difference between the modeled and measured components of emissivity are computed. An example of the resulting error surface is shown in Fig. 6. 5. The error surface is searched for local minima. Each local minimum represents a possible solution of the wind vector

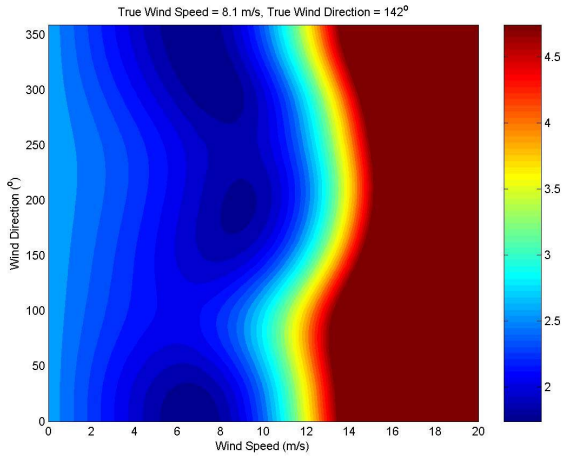

Fig. 6. Example surface of the cost function in (wind speed, wind direction) space that is minimized by the wind vector retrieval algorithm. Two local minima are present, representing two possible solutions.. The true wind vector, as determined by a coincident NDBC buoy, is (8.1 m/s, 142°).

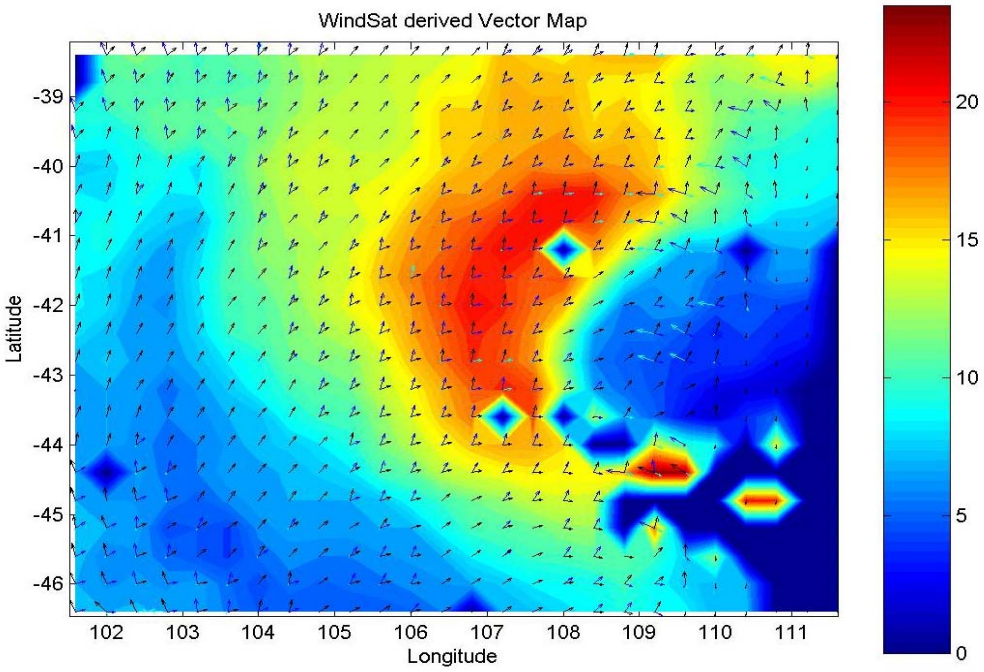

Fig. 7. Wind vector field retrieved by WindSat using an emissivity-based empirical model function, with multiple solutions included. Clockwise cyclonic organization is evident around the low.

retrieval algorithm. Two local minima are present in the figure, one at approximately (7 m/s, 320°) and the other at (9 m/s, 190°). A nearby NDBC buoy recorded wind speed and direction of (8.1 m/s, 142°) at approximately the time of the s/c overpass. An example of the wind vector image that is retrieved in this way is shown in Fig. 7. The background color describes the retrieved wind speed and direction is denoted by the arrows. Multiple solutions (i.e. multiple local minima) are shown as multiple arrows originating from a single point. A region of low pressure produces the clockwise rotation in this Southern hemisphere image. The darker arrows in the figure denote that solution with the lowest RMS difference between measured and modeled emissivities. This is the "first rank" solution. In most cases, the first rank solution appears to best capture the expected cyclonic rotation, suggesting that the skill of the retrieval is fairly high. However, this is not always the case and so some other method or methods of selection between the ambiguous wind vector solutions is needed. There have been numerous methods developed to address a similar characteristic of wind vector retrievals by radar scatterometers. Adaptation of those methods to the polarimetric radiometer case is an area of current research.

VI. SUMMARY

Calibration of the WindSat polarimetric radiometer has been evaluated in two ways. Using an electromagnetic model, the Antenna Pattern Correction algorithm has been updated to include a more accurate representation of the sidelobe structure of the radiation pattern. Calibration biases have been identified and characterized using a vicarious cold reference method. Cross-contamination between the V- and H-pol channels at 6.8 GHz has been identfied in this way. An ocean surface emissivity estimator has been has been developed to removes atmospheric contributions from the observed T_Bs. Using this estimator. empirical Geophysical Model Functions have been developed that relate the emissivity to ocean surface wind speed and direction at each WindSat frequency and polarization. A wind vector retrieval algorithm has been developed, based on this model function. Current and ongoing research is concentrated on characterizing and improving on the performance of this algorithm.

REFERENCES

Gaiser, P. (1998). WindSat Critical Design Review, Remote Sensing Division, Naval Research Laboratory, Washington, DC.

Ruf, C.S. (2000). "Detection of calibration drifts in spaceborne microwave radiometers using a vicarious cold reference," IEEE Trans. Geosci. Remote Sens., **38**(1), 44-52.

Yueh, S.H. (1997). Modeling of wind direction signals in polarimetric sea surface brightness temperatures. IEEE transactions on geosciences and remote sensing, **35**(6), 1400-1418

Yueh, S.H., W.J. Wilson, S.J. Dinardo, F.K. Li. (1999). Polarimetric microwave brightness signatures of ocean wind directions. IEEE transactions on geosciences and remote sensing, **37**(2), 949-959